PROTEINS
STRUCTURE ■ FUNCTION ■ BIOINFORMATICS

Holo-BtuF stabilizes the open conformation of the vitamin B12 ABC transporter BtuCD

Christian Kandt[1,2*] and D. Peter Tieleman[2]

[1] Department of Life Science Informatics B-IT, University of Bonn, 53113 Bonn, Germany
[2] Department of Biological Sciences, University of Calgary, Calgary, Alberta T2N 1N4, Canada

ABSTRACT

While there is evidence that other ABC transporters can tell between empty and loaded substrate binding protein, reconstitution experiments suggest otherwise for the *Escherichia coli* vitamin B12 importer BtuCD-F. Here, we address the question of BtuCD-F substrate sensitivity in a combined protein–protein docking and molecular dynamics simulation approach. Starting from the BtuCD and holo-BtuF crystal structures, we model two holo-BtuCD-F docking complexes differing by a 180° orientation of BtuF. One of these is similar to the apo-BtuCD-F crystal structure. Both docking complexes were embedded in a lipid/water environment to investigate their dynamics and BtuCD's conformational response to the presence and absence of BtuF, vitamin B12, and Mg-ATP in a series of 28 independent MD simulations. We find holo-BtuF stabilizing the open conformation of BtuCD, whereas the transporter begins to close again when BtuF or vitamin B12 is removed—suggesting BtuCD-F is capable of substrate sensitivity. We identified BtuC transmembrane helices 3 and 5, the L-loops and the adjacent helices comprised of BtuC residues 170–180 as hotspots of conformational change. We propose the latter to act as substrate sensors. BtuF-Trp44 appears to act as a lid on the vitamin B12 binding cleft in BtuF X-ray structures and protrudes into the BtuCD transport channel in one of our simulations, which might represent an initial step in vitamin B12 uptake. On an average, we observe subunit motions where the nucleotide binding domains approach each other while the transmembrane domains display an opening trend toward the periplasm.

Proteins 2010; 78:738–753.

Key words: molecular dynamics simulation; protein–protein docking; metabolite transport, membrane protein; model membrane; nutrient uptake; *Escherichia coli*; substrate sensitivity.

INTRODUCTION

ABC transporters are modular molecular machines found in all forms of life. Using the energy of ATP hydrolysis, they transport a broad range of substrates across biological membranes. Some ABC transporters, like the multidrug transporter P-glycoprotein[1,2] or the lipid-flippase MsbA,[3] receive their substrate from the lipid phase. Others like the maltose transport system $MalFGK_2$[4,5] or the vitamin B12 importer BtuCD-F[6,7] obtain their substrate from the aqueous phase, delivered by a specialized substrate binding protein (SBP). ABC transporters are medically relevant as their malfunction and/or overexpression accounts for a number of genetic diseases[8] and multidrug resistance of tumor cells or pathogenic bacteria.[9–11] Recent reviews on ABC transporters can be found in Refs. 2,9, and 11–18. At the time of writing, crystal structures have been determined for eight different full-length ABC transporters: BtuCD,[7] apo-BtuCD-F,[6] the structurally very similar HI1470/71,[19] the molybdate importer ModBC, with[20] and without SBP,[21] the maltose importer $MalFGK_2$ with maltose captured inside the transport channel,[5] the multidrug transporter SAV1866,[22,23] the methionine transporter MetNI,[24] P-glycoprotein[1] as well as Cα-trace structural models of the lipid flippase MsbA.[3]

All ABC transporters share a common architecture comprising two transmembrane domains (TMDs) that form the transport channel as well as two nucleotide binding domains (NBDs)—water soluble proteins associated with the TMDs on one side of the membrane. TMDs and NBDs together can consist of four subunits as described in Refs. 5,7,19–21, and 24, two as described in Refs. 3,22, and 23, or one continuous polypeptide chain as in P-glycoprotein.[1] The NBDs are the engines of an ABC transporter as they bind and hydrolyze ATP to power transport. Thereby, a cycle of conformational changes is induced that switches between different states of transporter accessibility. Although initially crystal structures of MalK and BtuCD suggested two possible coarse translocation mechanisms,[5,7,25] current ABC transporter crystal structures,[1,3,5–7,19–24] and simulation

Additional Supporting Information may be found in the online version of this article.
Grant sponsors: Canadian Institutes of Health Research, Alberta Heritage Foundation for Medical Research, Ministerium für Innovation, Wissenschaft, Forschung und Technologie des Landes Nordrhein-Westfalen (NRW Rückkehrerprogramm).
*Correspondence to: Christian Kandt, Computational Structural Biology, Department of Life Science Informatics, B-IT, Life and Medical Sciences (LIMES) Center, University of Bonn, Dahlmannstr 2, 53113 Bonn, Germany. E-mail: kandt@bit.uni-bonn.de.
Received 4 May 2009; Revised 19 August 2009; Accepted 26 August 2009
Published online 11 September 2009 in Wiley InterScience (www.interscience.wiley.com).
DOI: 10.1002/prot.22606

data[26] now point toward a scenario where NBD dimerization causes the TMDs to adopt an open-to-periplasm conformation. However, whether the actual power stroke in the transport cycle lies in the binding or hydrolysis of ATP or the release of ADP or comprise contributions of all three events is still under debate.[18]

BtuCD is the ABC transporter in the vitamin B12 uptake system in *Escherichia coli*. The outer membrane protein BtuB[27–29] shuttles vitamin B12 into the periplasmic space of the cell, where the substrate is received by the periplasmic SBP BtuF,[30,31] and subsequently delivered to the inner membrane ABC transporter BtuCD.[7] Apart from the BtuB, BtuF, and BtuCD components, the inner membrane protein TonB has been identified as another player in the uptake system crucial to vitamin B12 transport *in vivo*.[32] The exact details of how vitamin B12 is delivered to BtuCD are not fully understood yet.[28,33,34] The apo crystal structure of the BtuCD-F complex[6] shed light onto the organization of transporter and binding protein in the absence of vitamin B12 substrate or nucleotide. Beyond confirming the earlier postulated direct interaction of conserved surface BtuF glutamates and BtuC arginines,[30] the structure revealed interesting details concerning BtuCD open state and transporter—binding protein interaction. First, the apo-BtuCD-F crystal structure brought the first direct crystallographic observation of clear BtuF opening, thus confirming earlier predictions made in a BtuF simulation study.[35] Second, in the absence of BtuF and with vanadate trapped in between the NBDs, BtuCD was found accessible from the periplasm but closed on the cytoplasmic side.[7] Inserted in a POPE membrane/water environment, the 1L7V BtuCD structure has been reported to close within a few nanoseconds of MD simulation.[26,36] The vitamin B12-free 2QI9 BtuCD-F X-ray structure, however, is closed on both sides which has been interpreted as representing a post-transport state.[6] That closure is characterized by a tilted transmembrane helix (TM) 5 in one TMD subunit and two other TMD helices comprising BtuC residues 170–180 that extend deeply into the BtuF B12-binding cleft[6] [Fig. 2(a)]. In the following, we will refer to these helices as "sealing helices" (SH). As this configuration leaves no room for vitamin B12 to fit in the binding cleft [Fig. 2(b)], one can expect clear conformational differences between apo- and B12-bound BtuCD-F. Closed to both sides and with one TM-5 in tilted orientation, the apo-BtuCD-F X-ray structure represents a conformation half way between the BtuCD and HI1470/71 structures[7,19] that are open toward opposite sides of the membrane. The different open states seen in the BtuCD and apo-BtuCD-F structures along with the SH switching between a protruding and retracted orientation, could relate to the question of ABC transporter substrate sensitivity and if BtuCD represents a special case in this matter. While reconstitution experiments brought clear evidence for substrate sensitivity in maltose, histidine, and glycine betaine ABC transporters,[37–42] similar experiments suggested otherwise for BtuCD-F.[33] This was based on ATPase activity measurements, where the ABC transporters were studied with and without SBP and in the presence of SBP plus transport substrate. Except for BtuCD, the largest increase in ATPase activity was observed when SBP and transport substrate were provided simultaneously. In BtuCD, however, no difference in ATPase activity was observed regardless if BtuF was added alone or together with vitamin B12. This was interpreted as the vitamin B12 transporter being unable to tell between empty or B12-loaded BtuF.

ABC transporters have been studied computationally using both molecular dynamics simulation and normal mode analysis on full-length structures as well as isolated transporter components.[15,26,43–49] In this study, we address the question of BtuCD-F substrate specificity in a combined protein–protein docking and molecular dynamics simulation approach. The starting point of our simulations is a structural model of the vitamin B12-bound BtuCD-F complex. In the absence of a holo-BtuCD-F crystal structure, such a model can be obtained by modifying the apo-BtuCD-F X-ray structure[6] or by means of protein docking using the holo-BtuF[31] and BtuCD crystal structures.[7] Although work on the first approach is currently on the way in our laboratory, we here report the results obtained from the docking strategy. We carried out a series of BtuCD-F MD simulations monitoring BtuCD's conformational response to the presence and absence of BtuF, vitamin B12, and Mg-ATP on a time scale of up to 35 ns. Given that this is too short to obtain equilibrated complex structures and BtuCD has been reported closing within less than 10 ns in previous simulations,[26,36] we chose the transporter's response in open state as the main focus in our analysis to provide evidence for or against substrate sensitivity.

We find two possible B12-BtuCD-F docking complexes [Fig. 1(a,b)] whose dynamics in a palmitoyloleoyl-phosphatidyl-ethanolamine (POPE) membrane/water environment were studied in a series of 28 independent multicopy MD simulations[50] [Fig. 1(c)]. Ten simulation scenarios were considered characterized by the presence or absence of BtuF, vitamin B12, and Mg-ATP. We simulated both complexes with and without Mg ATP in a series of 12 independent simulations (total of 300 ns simulation time), followed by additional 10 BtuCD continuation runs—with and without Mg ATP—(150 ns in total) to investigate the effect of BtuF removal. Finally, we performed another six MD runs of apo-BtuCD-F (185 ns total simulation time)—with and without Mg ATP—to test how vitamin B12 itself influences the transporter open state. To investigate the possibility of force field dependency, we additionally performed the apo-BtuCD-F simulations using a different force field (Supporting Information materials). We find holo-BtuF stabilizing a

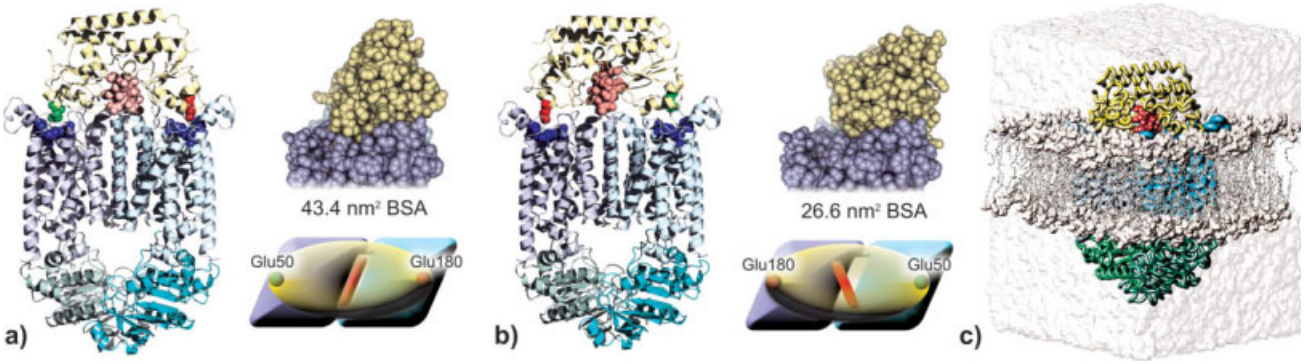

Figure 1

Using conserved surface glutamate (green, red) and arginine (blue) residues as guideline, two BtuCD-F docking complexes were obtained (**a**, **b**) differing by a 180° rotation of BtuF (yellow). The cartoons in (a, b) illustrate the different BtuF orientations. The BtuF-TMD buried surface area (BSA) is larger in complex 1 (a) and vitamin B12 is in an antiparallel alignment in respect to the TMD B12-uptake cleft in complex 2 (b). Both complexes were inserted into a POPE lipid bilayer patch (**c**) and simulated in a series of 28 MD simulations in the presence and absence of BtuF, vitamin B12, and Mg ATP.

BtuCD conformation that is open toward the periplasm. When binding protein or vitamin B12 is removed, the transporter begins to close again, suggesting that BtuCD is capable of substrate sensitivity. We analyzed the changes occurring at the subunits interfaces and monitored subunit rearrangements, which support a model of ABC transporter functional mechanism where NBD dimerization is concurrent with a transition of the TMDs toward an outward facing conformation. BtuCD transmembrane helices 3 and 5 and the adjacent sealing helices were identified as hotspots of conformational changes in the TMDs which may be involved in transporter gating, interdomain communication and substrate recognition. We propose the SH to act as substrate sensors. While BtuF Trp-44 appears to act as a lid on the vitamin B12 binding cleft in BtuF X-ray structures,[7,31] Trp-44 protrudes into the presumed TMD transport channel in one of our simulations which might represent an initial step in vitamin B12 uptake.

MATERIALS AND METHODS

Protein–protein docking

The 1L7V BtuCD[7] and 1N4A BtuF[31] crystal structures were used for docking. For the BtuCD-BtuF docking interface, the conserved surface residues Glu50 and 180 (BtuF) and Arg56, 59, 296 (BtuC) have been proposed as key elements.[30] These residues were used as a guideline and quality criterion during the docking process. In a first step, the online server version of ZDock[51,52] was used to generate a preliminary docking complex with the docking partners in a position consistent with the Glu/Arg locations. Negative docking constraints were applied to exclude surface residues from the docking interface facing either the lipid or cytoplasmic water phase (BtuC) or the periplasm (BtuF). In a second step, HeX 3.1[53] was used to perform a limited docking search around the preliminary ZDock complex, only allowing a restricted range of BtuF rotation and translation. The following HeX settings were applied: Search mode: orbit ligand; Correlation type: shape only; Radial filter: re-entrant; Post processing: BB-bumps; Ligand range: 45°, Twist range: 30°; Distance range: 30 Å; and Grid dimension: 0.4. Identification of a possible BtuC-F docking complex was based on a 4.5 Å BtuF-Glu–BtuC-Arg minimum distance cutoff. Since the BtuC subunits are identical, there are at least two possible BtuF orientations fulfilling the criterion of having the BtuF glutamates in interaction distance with the BtuC arginine clusters. Therefore, the first possibility was modified by manually rotating BtuF by 180° around the *z*-axis. Subsequently, a second HeX and minimum Glu–Arg distance search was performed using the same settings as before.

Simulation setup

Molecular dynamics simulations were performed using the GROMACS 3.3.1 package and ffgmx force field.[54,55] The force field parameters used for vitamin B12 have been described in Ref. 35. The two vitamin B12 bound BtuCD-F complexes generated in the protein–protein docking [Fig. 1(a,b)] were used as starting structures. Initially four different simulation systems were created: each of the two docking complexes with and without magnesium ATP. The nucleotide-bound form of BtuD was adapted from Ref. 36. The protein was inserted into a pre-equilibrated POPE bilayer using INFLATEGRO as detailed in Ref. 56. The final simulation systems [Fig. 1(c)] comprise 1354 protein residues, 1 vitamin B12, 326

Table I
Simulation Scenarios and Runs

Scenario	Simulations	Simulation time	
B12-BtuCDF	Complex 1	3× 20 ns no ATP	3× 20 ns Mg ATP
	Complex 2	3× 30 ns no ATP	3× 30 ns Mg ATP
$BtuCD_{continuation}$	Complex 1	2× 10 ns no ATP	2× 20 ns Mg ATP
		1× 10 ns no ATP	1× 10 ns Mg ATP
	Complex 2	1× 20 ns no ATP	1× 20 ns Mg ATP
		2× 10 ns no ATP	
Apo-BtuCD-F	Complex 1	3× 30 ns no ATP	2× 30 ns Mg ATP
			1× 35 ns Mg ATP
Apo-BtuCD-F G53a6	Complex 1	3× 30 ns no ATP	2× 30 ns Mg ATP
			1× 35 ns Mg ATP

POPE lipids, and 34,300 simple point charge water molecules.[57] Depending on the presence or absence of magnesium ATP, 17 or 21 chloride ions were added to neutralize the system's net charge. Standard protonation states were assumed for titratable residues.

Similar as in Ref. 50, a series of multiple independent MD simulations were performed, where for each system three production runs were initiated using a different temperature seed number to generate the random distribution of starting velocities (Table I). The simulations started with 1 ns membrane equilibration during which protein, vitamin B_{12}, and nucleotides were position-restrained, applying a force constant of 1000 kJ mol^{-1} nm^{-2}.

In two consecutive 10 ps simulations, position restraints were used where the force constants were first lowered down to 100 and then to 10 kJ mol^{-1} nm^{-2} in the second run. Position restraints were deactivated for the production runs. Three main simulation scenarios where considered, each with and without Mg ATP (Table I): (1) Twelve individual holo-BtuCD-F production runs were performed, with simulation times of either 20 or 30 ns. (2) In 10 cases, BtuCD continuation runs were carried out prior to which BtuF and vitamin B12 had been removed. Box sizes were adjusted and re-solvated with 21,900 SPC water molecules. Depending on the presence or absence of magnesium ATP, 16 or 20 chloride ions were added to neutralize the system's net charge. After energy minimization, the BtuCD continuation systems were simulated for either 10 or 20 ns. (3) For complex 1, six further simulations were performed using the same starting structures as in holo-BtuCD-F but removing vitamin B12 prior to solvation with SPC water and 17 respective 21 chloride ions. Analogue to the holo-BtuCD-F simulations, production runs were preceded by 1 ns membrane equilibration and two consecutive 10 ps runs to release the position restraints on protein and nucleotides. Apo-BtuCD-F simulations were 30–35 ns long.

In the simulations, all bond lengths were constrained by LINCS so that an integration time step of 2 fs could be used.[58] Systems were simulated at a temperature of 310 K, maintained separately for water + ions and protein + vitamin B12 + nucleotides by a Berendsen thermostat[59] with a time constant of 0.1 ps. A Berendsen barostat[59] was applied using semisotropic pressure coupling with time constants of 1 ps and reference pressures of 1 bar for the contributions in Z- and XY-directions. Electrostatic interactions were calculated using particle mesh Ewald summation[60,61] and twin range cutoffs of 0.9 and 1.4 nm were applied for computing the van der Waals interactions.

To test for possible force field dependencies, the six apo-BtuCD-F simulations were repeated using the G53a6-GROMOS96 force field.[62] These simulations were performed with GROMACS 4.0.3[63] using the same simulation settings as mentioned earlier.

Analysis

To compare the docking complexes before and after each simulation scenario with the available crystal structures, the entire complexes as well as the individual domains were superimposed on the apo-BtuCD-F crystal structure 2QI9 and corresponding Cα-RMSDs were computed. The BtuCD crystal structure 1L7V was also included in this comparison. This was carried out in PyMol (Fig. 2).

The transporter open state was monitored using two different approaches: (1) Similar to the mean water densities in Refs. 64 and 65, mass-weighed protein densities (MPDs) averaged over the last 5 ns of each BtuCD-F trajectory were calculated using the VolMap tool in VMD 1.8.5 and 1.8.6.[66] Voxel size was set to 1 $Å^3$, and the protein atoms' van der Waals radii were taken into account. The presented volume slices in the plane of the membrane normal display for each trajectory the maximum BtuC opening toward BtuF. (2) TMD-TMD interface residues were identified and visualized as trajectory snapshots in overlay with the end conformation of the TMD-1 subunit. TMD-interface residues were identified based on a 4 Å TMD-TMD distance cutoff over the last 5 ns of each trajectory.

Changes in the BtuF-TMD and TMD-TMD interface region were monitored by computing their buried surface area (BSA) as a function of time. To this end, NACCESS 2.1.1[67] was used to calculate the solvent accessible surface area S of two neighboring subunits A and B, both individually S(A), S(B), and together S(AB). S(A) + S(B) minus S(AB) then yields the BSA. Contact interfaces between BtuF and TMD subunits were further characterized by minimum distance analyses, time- and run-averaged over the last 5 ns of each trajectory.

The tilt angle between the main principle axes of inertia of each trans membrane unit was computed in VMD as outlined in Ref. 26. To identify hotspots of conformational change in the TMDs in terms of secondary structure elements, C_α root mean square deviations per α-helix were computed between the energy-minimized starting structure and the end conformation of each run.

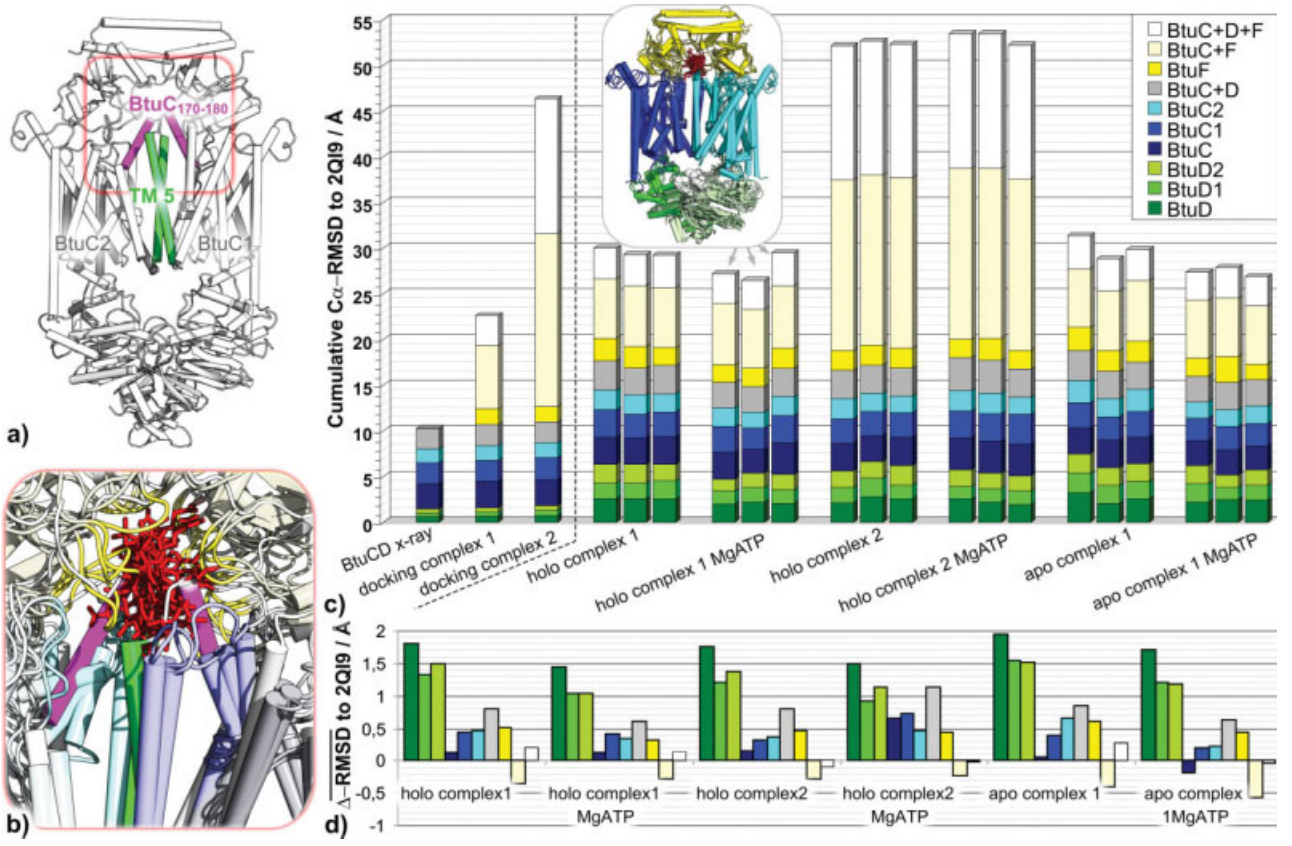

Figure 2

The BtuCD-F crystal structure (**a**) features a singular BtuF orientation and was solved in absence of vitamin B12 or nucleotides. Beyond that, the major difference to our simulation structures lies in the tilted orientation of one transmembrane helix (TM 5) in the TMD-1 subunit, and two adjacent non-TM helices ($BtuC_{170–180}$) protruding deeply into the BtuF binding cleft. As illustrated by an overlay with holocomplex 1 end conformations, this configuration leaves no room for vitamin B12 to fit in the binding cleft (**b**). To compare the X-ray structure with simulation start and end conformations, Cα-RMSDs of the entire complex and its subunits were calculated (**c**). Each conformation is represented by a single bar comprising several segments whose lengths reflect the complex subunits' Cα-RMSD to the X-ray structure. The segments are color-coded by BtuCD-F subunits as illustrated by the inset of simulation end structures. As indicated by the averaged Cα-RMSD changes between simulation start and end structures, only small conformational changes occur that do not exceed 2 Å (**d**). Most changes happen in the NBDs.

This was carried out for a subset of TMD-C_α atoms that were identified in RasMol 2.7.2[68] as α-helical in the BtuC crystal structure.[7] After averaging over the three independent copies of each of the three simulation scenarios, the RMSDs were mapped onto the energy-minimized starting structures for visualization.

RESULTS

Protein–protein docking

Two possible BtuCD-F docking complexes were obtained. Both have the conserved surface glutamates and arginines of periplasmic binding protein and BtuC transmembrane units within 4 Å interacting distance as proposed in Ref. 30. However, the complexes have a different BtuF orientation: while in complex 1 BtuF-Glu50 is interacting with the arginine cluster of BtuC subunit A [Fig. 1(a)], in the second complex Glu50 interacts with the arginines of BtuC subunit B [Fig. 1(b)]. As a result of the different BtuF orientation in complex 1 vitamin B12 is in a parallel alignment with respect to the presumed substrate uptake cleft between the BtuC subunits, but not in complex 2. Furthermore, the BtuC-BtuF contact interface—as determined by the BtuC-F BSA—is smaller in the second BtuCD-F complex (26.6 nm^2) than in the first one (43.4 nm^2). Compared with the apo-BtuCD-F X-ray structure, the docking complexes yield Cα-RMSDs of 3.2 Å (complex 1) and 14.7 Å (complex 2) after structural alignment in PyMol[69] [Fig. 2(c)]. The BtuC–BtuF contact interface in the crystal structure is 53.1 nm^2.

Simulation and X-ray

The apo-BtuCD-F crystal structure was solved without vitamin B12 or nucleotide. Next to a singular BtuF orien-

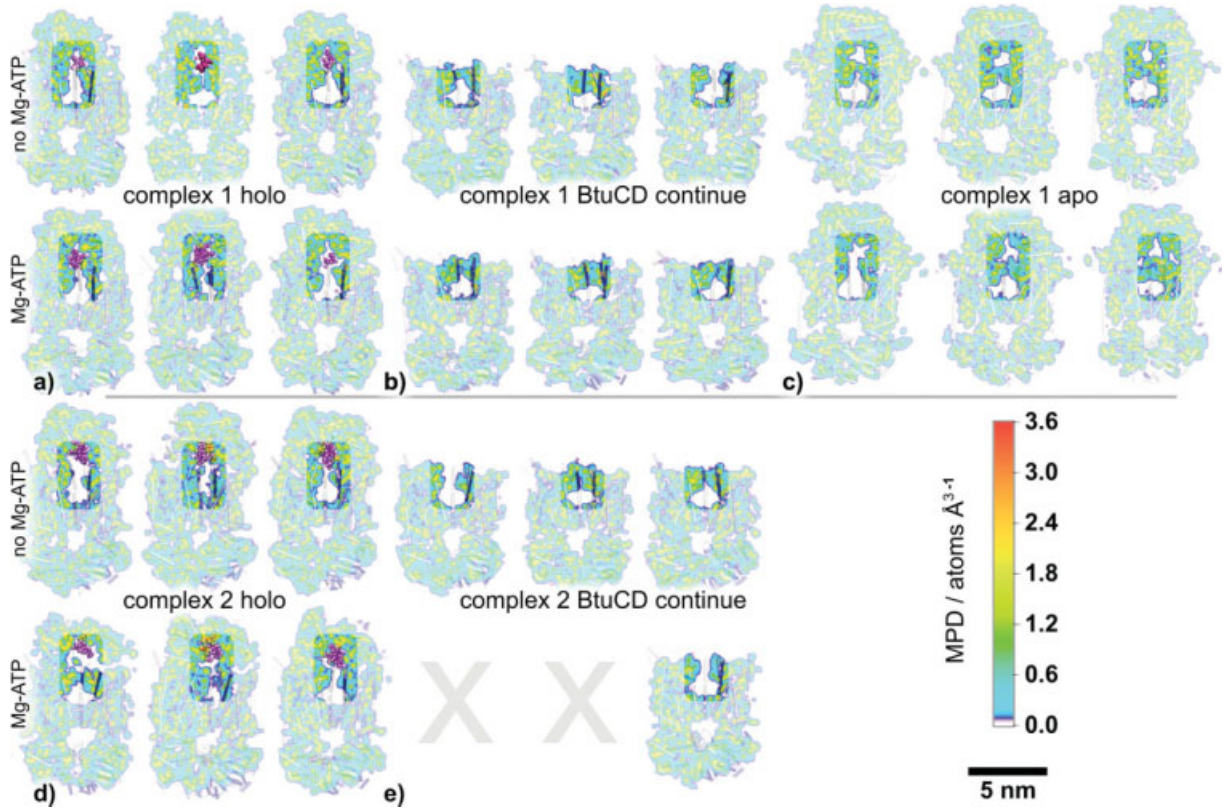

Figure 3

Slices through mass-weighed protein densities (MPD) averaged over the last 5 ns of each trajectory. The density data was recorded for all nonhydrogen atoms of each of the holo (**a**, **d**), BtuCD continue (**b**, **e**) and apo (**c**) simulations. The periplasmic entrance region of BtuCD is highlighted.

tation, the main difference between simulation and crystal structure lies in the BtuCD open state. The crystal structure[6] is closed on both sides which is due to TM 5 in the BtuC-1 subunit and the SH conformation in both BtuC protomers [Fig. 2(a)]. The SH protrude deeply into the BtuF substrate-binding cleft where they would clash with vitamin B12 if any were present [Fig. 2(b)]. As highlighted in the same figure, BtuC-1 TM5 is in a tilted orientation that is comparable with the one seen in both TMD units in HI1470/71.[19]

To quantify conformational differences between the apo-BtuCD-F X-ray structure and the docking complexes before and after simulation, Cα-RMSDS were computed for the entire complex and individual subunits [Fig. 2(c)]. Initially, the two docking complexes are as different from 2QI9 apo-BtuCD-F as the 1L7V BtuCD X-ray structure, which was used to build them. The largest deviations are seen in the BtuC-F (6.9 Å for complex 1 and 18.9 Å for complex 2) and BtuCD-F RMSD (3.2 Å for complex 1 and 14.7 Å for complex 2) reflecting the different BtuF orientations in the docking complexes. The orientation in complex 1 is similar to the one found in the apo-BtuCD-F crystal structure. Beyond that, the docking complexes differ by 2.8 Å in their TMD RMSD from apo-BtuCD-F due to the tilted TM5 helix in the BtuC-1 subunit. In all simulation scenarios only small conformational changes occur on the Ca-RMSD level, which do not exceed 2 Å [Fig. 2(d)]. Most changes occur in the NBDs (ΔRMSD 1.4–1.9 Å) while in all other components the change in RMSD is smaller than 1 Å. The ΔRMSDs in the NBDs are slightly bigger (by 0.3–0.6 Å) in the NBD dimer than in the individual monomers. Furthermore, the NBD RMSD change is smaller when Mg-ATP is present. With 0.3–0.6 Å these differences are small but are seen in all three complex simulation scenarios.

Transporter open state

To investigate how the presence of docked BtuF and vitamin B12 substrate affects the open state of BtuCD, we calculated MPDs averaged over the last 5 ns of each trajectory (Fig. 3) and identified TMD interface residues that are within 4 Å of each of the TMD subunits during the last 5 ns of each trajectory (Fig. 4).

Figure 3 shows slices through the protein densities, each displaying the maximum open state of BtuCD.

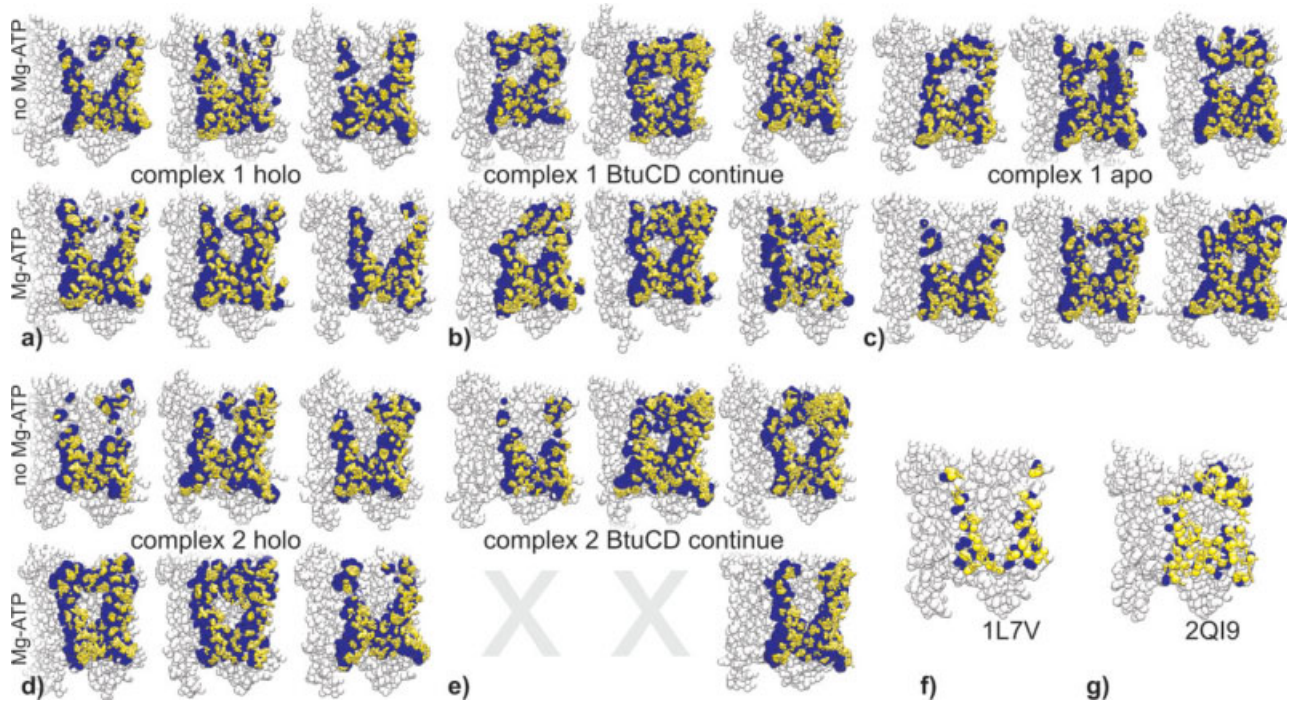

Figure 4

TMD-TMD interface residues in the simulation (**a**–**e**) and the BtuCD (**f**) and BtuCD-F (**g**) X-ray structures. TMD-1 residues that are within 4 Å of TMD-2 appear blue, TMD-2 residues within 4 Å of TMD-1 are yellow. The white subunit is the TMD-1 end conformation with interface residues shown as overlay of simulation snapshots over the last 5 ns of each trajectory.

Based on the MPDs, after the holo-BtuCD-F simulations, BtuCD is in an open conformation in 5/6 runs [complex 1, Fig. 3(a)] and 4/6 runs [complex 2, Fig. 3(d)]. When the substrate-bound BtuF is removed from the end structures of the open BtuCD-F complexes and BtuCD continuation runs are carried out, BtuC closes within 10–20 ns in 5/6 simulations of complex 1 [Fig. 3(b)] and in two of four cases for complex 2 [Fig. 3(e)]. When the complex 1 simulations are repeated without vitamin B12, the transporter again adopts a closed conformation in 5/6 cases after 30–35 ns [Fig. 3(c)]. Using GROMACS 4 and the G53a6-GROMOS96 force field, apo-BtuCD-F adopts a closed conformation in 6/6 cases (Supporting Information Figure S1).

The TMD interface analysis (TIA) (Fig. 4) generally confirms the findings of the MPD analysis except for one nucleotide-free run of the holo-complex 1 simulations. Apparently closed in the MPD [Fig. 3(a)], it is found open in the TIA [Fig. 4(a)]. While the MPD slices can only be shifted along the *x*-, *y*- or *z*-axes, TIA explicitly identifies interface residues thus additionally providing information on the shape of the presumed transport channel which varies between straight up toward the periplasm, and wide open as in [Fig. 4(a) both rows, right; Fig. 4(c) lower row, left; Fig. 4(e) upper row, left] and narrow and tilted as in [Fig. 4(a) lower row, middle; Fig. 4(d) upper row, middle].

TMD and NBD orientations

Changes in the orientation of TMD and NBD subunits were monitored by computing the tilt angle between the TMDs principle axis of inertia and center of mass (COM) distances between NBDs and L-loops. Located at the TMD-NBD interface, the L-loops are formed by two small non-TM helices and are generally thought to sense and propagate rearrangements of the NBDs to the TMDs of many ABC transporters.[11,16] The time- and run-averaged distance and angle changes during the BtuCD-F simulations are given in Figure 5.

In all BtuCD-F simulations, the NBD COM distance decreases [Fig. 5(a)]. The NBDs approach each other by an average of 1 Å (holo-C2 Mg ATP) up to 1.5 Å (apo-C1 no Mg ATP and holo-C1 Mg ATP). Standard deviations range from ±0.2 Å (apo-C1 Mg ATP) to ±0.7 (holo-C1 no Mg ATP). L-loop distances increase in the holosimulations and decrease slightly in the aporuns [Fig. 5(b)]. Observed distance changes range from −0.4 Å (apo-C1 Mg ATP) to 3.1 Å (holo-C2 Mg ATP). The distance changes exhibit strong fluctuations throughout

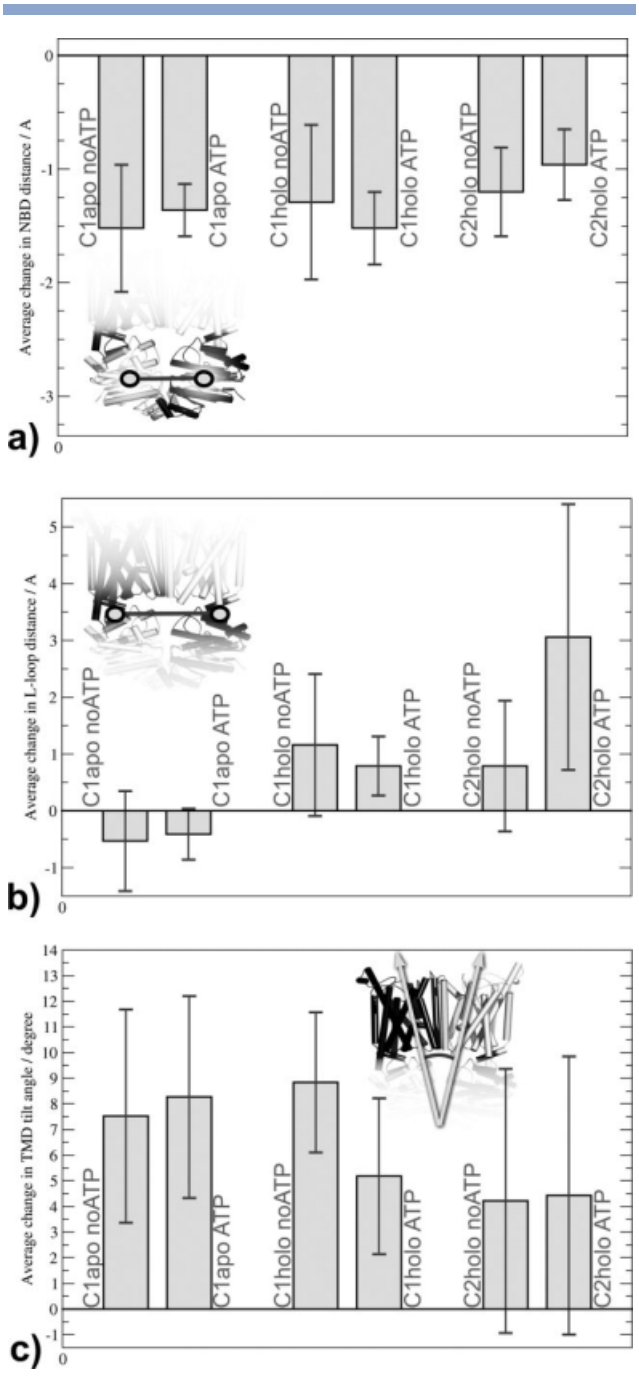

Figure 5

Rearrangements of the nucleotide binding and transmembrane domains as monitored by the time and run-averaged changes in NBD (**a**) and L-loop (**b**) center of mass distance as well as the tilt angle of the principle axes of inertia of the TMDs (**c**). On an average, the NBDs come closer together whereas at the same time the tilt angle between the TMDs increases. Changes in the L-loop distance do not appear to be coupled to this.

the independent copies of each simulation system, ranging from ±0.4 Å (apo-C1 Mg ATP) up to ±2.3 Å (holo-C2 Mg ATP). The tilt angle between TMD subunits' main principal axes of inertia increases in all BtuCD-F simulations [Fig. 5(c)]. Average angle changes range from 4.2° (holo-C2 no Mg ATP) to 8.8° (holo-C1 no Mg ATP). Again distinct fluctuations occur throughout the independent simulation copies, producing standard deviations between ±2.7° (holo-C1 no Mg ATP) and ±5.4° (holo-C2 Mg ATP).

TMD hotspots of conformational change

For the BtuCD-F simulations, we calculated Cα root mean square displacement per α-helix to identify hotspots of conformational change in the TMDs of holocomplex 1 [Fig. 6(a,b)], holocomplex 2 [Fig. 6(c,d)], and apocomplex 1 [Fig. 6(e,f)]. Helix RMSDs were averaged over the end structures of the three independent copies of each simulation system and visualized in two ways: (1) as RMSD versus residue plots [Fig. 6(a,c,e)] and (2) helices exceeding 2 Å RMSD highlighted in context of the BtuCD X-ray structure [Fig. 6(b,d,f)].

Helix RMSDs range from 0.6 Å [TM2 in MgATP apocomplex 1, Fig. 6(e)] up to 3.6 Å [sealing helix in nucleotide-free holocomplex 1, Fig. 6(a)]. While most helices display RMSDs in a range of 1–1.5 Å, the largest conformation changes concentrate on a few single α-helices. For holocomplex 1, these are TM5, TM3, the L-Loops and the sealing helices (SH) [Fig. 5(a,b)]. In the complex 2 simulations maximum TMD changes occur at TM5, TM3, L-loops, SH, and TM10 [Fig. 6(c,d)]. In apo-BtuCD-F maximum conformational changes concentrate on TM5, TM3, SH, and L-loops [Fig. 6(e,f)]. Overall, the hotspot helices show an asymmetric distribution concentrating on TMD subunit A.

Changes at the BtuF and TMD interfaces

BtuF-TMD contact interface

Changes in the BtuF-TMD interface were characterized by computing the BSA between BtuC and BtuF (Fig. 7) and monitoring the residues in the docking interface (Table II).

In all BtuCD-F simulations, the BtuF-TMD interface area increases, with observed changes ranging from 37.3 nm^2 (holo-C2 Mg ATP) up to 62.5 nm^2 BSA (apo-C1 no Mg ATP) [Fig. 7(a)]. Five of the holo-C1 simulations reach end BSA values clustering around 50 nm^2 and as such are approximately half-way in between the initial BSA of 43.4 nm^2 in complex 1 and 54.4 nm^2 in the apo-BtuCD-F crystal structure. One nucleotide-free holo-C1 run yields an end BSA of 56.3 nm^2. Two of the holo-C2 simulations stay below the initial BSA in complex 1 (37.3 and 40.9 nm^2), three slightly surpass it (44.4 nm^2), while one nucleotide-free simulation reaches an end value of 50.5 nm^2. Except for one nucleotide-free run (49.8 nm^2), in all complex 1 aposimulations the BtuF-TMD BSA reaches end values equal to (one Mg ATP simulation) or exceeding the apo-

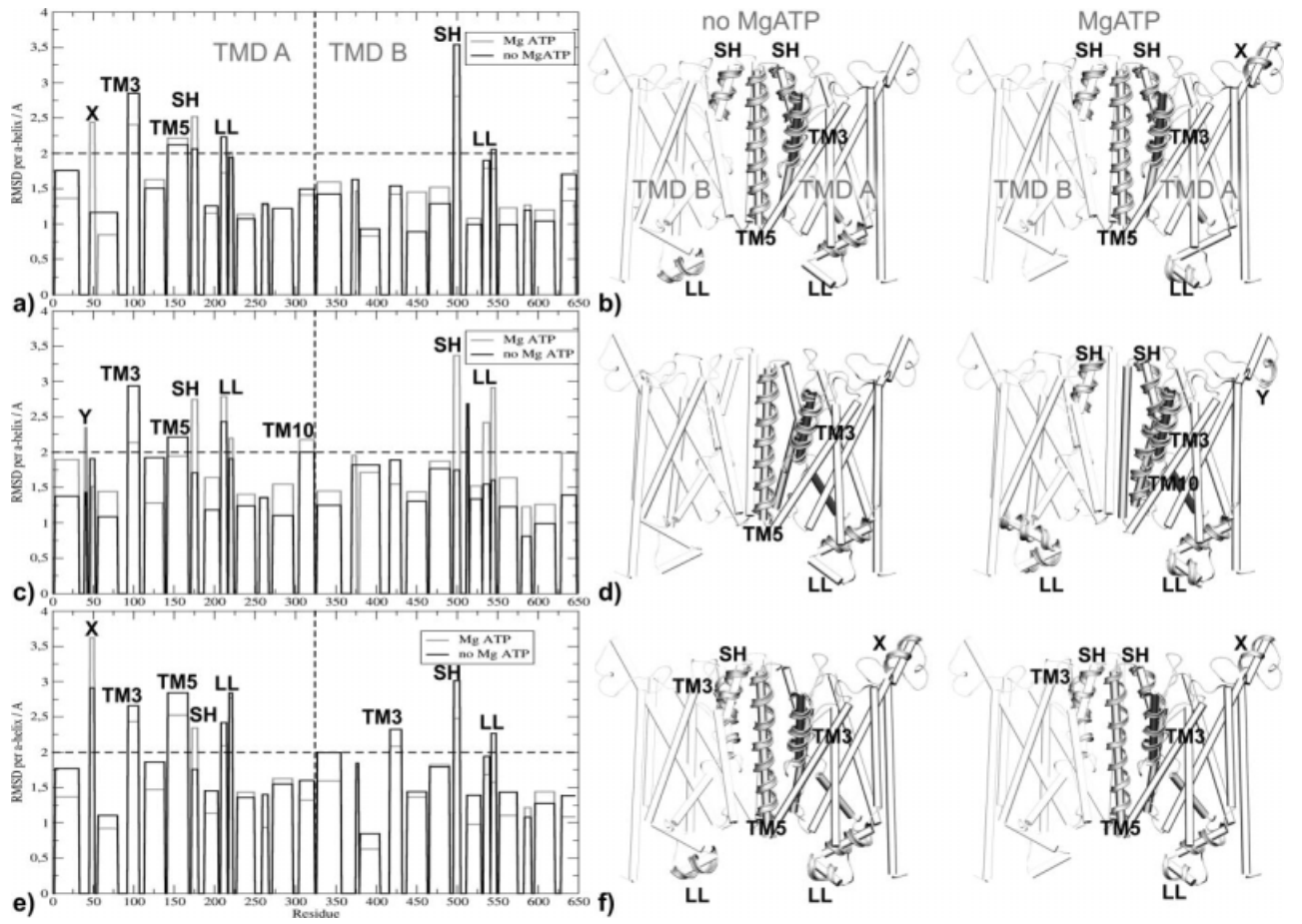

Figure 6

Hotspots of conformational change in the TMDs as determined by RMSD per α-helix averaged over the simulation end structures of holocomplex 1 (**a**, **b**), holocomplex 2 (**c**, **d**), and apocomplex 1 (**e**, **f**). Results are shown for all α-helices in (a, c, e), whereas hotspot helices are highlighted in context of the energy-minimized starting structures (b, d, f). Next to the L-loops (LL) hotspot helices include transmembrane helices 3, 5, 10 (TM3, TM5, TM10) and the sealing helices (SH) comprising BtuC residues 170–180. X denotes the first seven residues of TM2 RasMol and VMD identify as separate α-helix in TMD subunit A. Likewise, Y is a three residue section of the TM1–2 loop that adopts an α-helical configuration in TMD-A of complex 2.

BtuCD-F crystal structure (up to 62.5 nm^2 in a nucleotide-free simulation. In all three BtuCD-F simulations, the largest BtuF-TMD contact interface area occurs in nucleotide-free runs. At the same time, the TMD-TMD contact interface areas mainly lie between the complex 1/2 initial value of 26.7 nm^2 and 37.9 nm^2 in the apo-BtuCD-F X-ray structure [Fig. 7(b)]. At the end of the simulations, the lowest TMD interface area is observed in a nucleotide-free run of holo-C1 (25.9 nm^2), whereas the largest occurs in an Mg ATP run of apo-C1 (36.7 nm^2).

Residues in the BtuF-TMD interface

To identify the residues involved in BtuF-TMD interaction, time and run-averaged minimum distance analyses were carried out for each of holo- and apo-BtuCD-F simulations and the apo-BtuCD-F X-ray structure (Table II). In the following the term "interface residues" will be used synonymous to residues of one subunit which are located within 4 Å distance of the other subunit.

Reflecting the different starting BtuF-TMD interfaces of the initial docking complexes, complex 1 has 41 BtuF and 46 TMD interface residues, whereas only 24 BtuF and 27 BtuC interface residues are observed for complex 2. The apo-BtuCD-F crystal structure comprises 45 BtuF and 55 TMD interface residues. During the simulations, the average number of interface residues increases in both complexes regardless whether Mg ATP or vitamin B12 is present or not. After the simulations, the amount of interface residues ranges from 51 BtuF and 68 TMD residues (holo-C2 Mg ATP) to 63 BtuF and 79 TMD residues (holo-C1 no Mg ATP).

To address how many interface residues the three BtuCD-F simulations and the apo-BtuCD-F crystal struc-

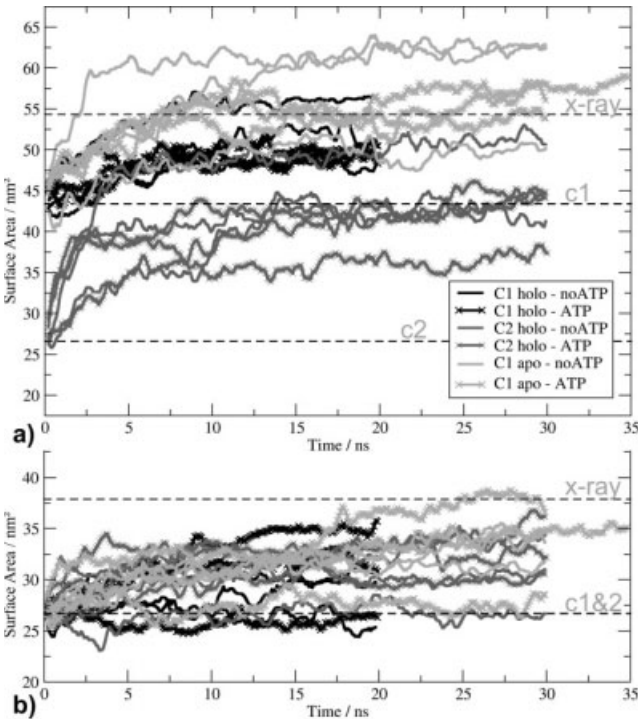

Figure 7

Buried surface area versus time as monitored for the BtuF-TMD (**a**) and TMD-TMD interface (**b**). The dotted lines indicate simulation starting values and the surface area in the apo-BtuCD-F crystal structure.

ture have in common, we calculated the percentage interface residues our simulation structures have in common with the holo-C1 complex structures and the apo-BtuCD-F crystal structure (Table III). Although in the beginning the C1 and C2 docking complexes share only 54% BtuF and 50% TMD interface residues, their amount increases to up to 84% BtuF and 76% TMD (holo-C2 no Mg ATP) and 87% BtuF and 90% TMD interface residues (apo-C1 no Mg ATP). Although prior to the simulations 66% of the BtuF and 70% of the TMD complex 1 interface residues are the same as in the crystal structure, these values decrease to 58% BtuF and 60% TMD residues at the end of the holo-C1 Mg ATP simulations. At the same time all holo- and apo-BtuCD-F simulations share more than 80% of the interface residues after starting from initial values of 60% BtuF and 58% TMD (complex 1) and 51% BtuF and 40% TMD interface residues (complex 2).

BtuF Trp44

Trp44 adopts different orientations in the apo- and holo-BtuF X-ray structures: While facing toward vitamin B12 in holo-BtuF 1N4A[31] and pointing away from the B12-binding cleft in apo-BtuF 1N4D,[31] in the apo-BtuCD-F complex 2QIJ,[6] Trp44 again faces the now empty B12-binding cleft but adopts a more inward-facing conformation [Fig. 8(a)]. In one of the Mg ATP-free runs of complex 1, BtuF Trp44 penetrates deeply into the putative BtuC translocation channel [Fig. 8(b)]. Although in 11 of 12 cases, the Trp44-BtuF and Trp44-BtuC COM-distances in the holo-C1 simulations fluctuate between 13.5 and 16.5 Å and 22 and 25 Å respectively, we observe a different behavior during the aforementioned nucleotide-free simulation. Here, the Trp44-BtuF COM-distance steadily increases from 15 to 19 Å, while at the same time the Trp44-TMD COM-distance decreases from 23.5 to 19 Å [Fig. 8(b)]. For the holo-C2 simulations one similar event, also in a nucleotide-free simulation, is observed. Here, the Trp44-BtuF and Trp44-BtuC COM distance transiently reaches a value of 19.5 and 21 Å respectively at 5 ns. However, the Trp44 does not intrude as deeply as it does in complex 1 and eventually relaxes back to 17 Å (Trp44-BtuF) and 24 Å (Trp44-TMD) during the remaining 25 ns simulation time17 Å (Trp44-BtuF) [Fig. 8(c)]. In the other 11 cases, the Trp44 conformation is characterized by COM distances of 14.5–16.5 Å (Trp44-BtuF) and 23–26 Å (Trp44-TMD). In the apo-C1 simulations, the Trp44 orientation displays greater fluctuations in the COM distances ranging from 12 to 18 Å (Trp44-BtuF) and 19 to 28 Å (Trp44-TMD) [Fig. 8(d)]. Again a transient intrusion into the TMD channel is observed during one of the nucleotide-free runs.

Table II

Average Number of Residues in the BtuF–BtuCD Docking Interface Before and After the Simulations, Averaged over the Last 5 ns of All Copies of Each Simulation

	C1 holo		C2 holo		C1 apo		X-ray	
Residues	BtuF	TMD	BtuF	TMD	BtuF	TMD	BtuF	TMD
Start	41	46	24	27	41	46	45	55
No Mg ATP	63	79	55	71	62	77		
Mg ATP	62	76	51	68	62	74		

Table III

Percentage of Interface Residues Our Simulation Structures Have in Common with the Holo-complex 1 (C1 holo) Structures and the Apo-BtuCD-F Crystal Structure

	C1 holo		C2 holo		C1 apo		X-ray	
	BtuF	TMD	BtuF	TMD	BtuF	TMD	BtuF	TMD
% of C1 holo								
Start	100	100	54	50	100	100	66	70
No Mg ATP	100	100	84	76	87	90	59	60
MgATP	100	100	71	75	90	84	58	60
% of X-ray								
Start	60	58	51	40	60	58	100	100
No Mg ATP	82	85	84	81	91	82		
MgATP	80	84	82	82	87	84		

Values are given before and after the simulations with and without Mg ATP.

DISCUSSION

Two complex structures

In this study, we addressed the question how vitamin B12 and BtuF affect the transporter open state and if BtuCD is capable of substrate sensitivity and can tell between empty and B-12 loaded BtuF. This was done using a combination of protein–protein docking of the BtuCD[7] and B12-bound BtuF crystal structures[31] and a subsequent series of 28 independent MD simulations. Given the availability of the apo-BtuCD-F crystal structure,[6] the question arises why we used holo-BtuCD-F models for our simulations that were built based on protein docking instead of using the B12-free complex structure as a template. On one hand, holo-BtuCD-F cannot be modeled by simply inserting vitamin B12 into the apo-BtuCD-F crystal structure, as the SH residues of the TMDs occupy more than half of the BtuF B12 binding cleft, leaving no room for vitamin B12 to fit in [Fig. 2(a,b)]. Another option would be a perturbation run strategy where vitamin B12 is slowly grown in its BtuF binding cleft and the complex structure is then given sufficient simulation time to adjust and equilibrate accordingly. However, this approach is technically challenging given that the post-transport conformation of the apo-BtuCD-F crystal structure[6] requires further modifications toward conformations as in Refs. 7 and 31 to correctly model a pretransport state. These modifications include retraction of the BtuF-protruding SH, re-closing of BtuF that has opened up by 5 Å as well as re-tilting of TM5 in BtuC-1. Although we are currently working on a holo-BtuCD-F model based on the apo-BtuCD-F X-ray structure, here we report results of our first holo-BtuCD-F structural models derived from protein–protein docking.

We found two possible holo-BtuCD-F docking complexes differing by a 180° rotation of BtuF (Figs. 1 and 2). Complex 1 features a better alignment of vitamin B_{12} with the BtuC substrate uptake cleft and a larger BtuC-F contact interface area as in complex 2. Both complexes have the conserved surface BtuF glutamates and BtuC arginines within 4 Å interaction distance as proposed in Ref. 30, and both were used as starting structures for the MD simulations. A first BtuCD-F docking complex was reported in Ref. 47, where a manual approach was used to bring the conserved surface BtuF glutamates and BtuC arginines in close proximity as proposed in Ref. 30. Vitamin B12 was not included in that study and the complex was assembled from BtuCD and BtuF simulation structures based on the respective crystal structures. The achieved docking orientation of BtuF in respect to BtuC was not specified. In our

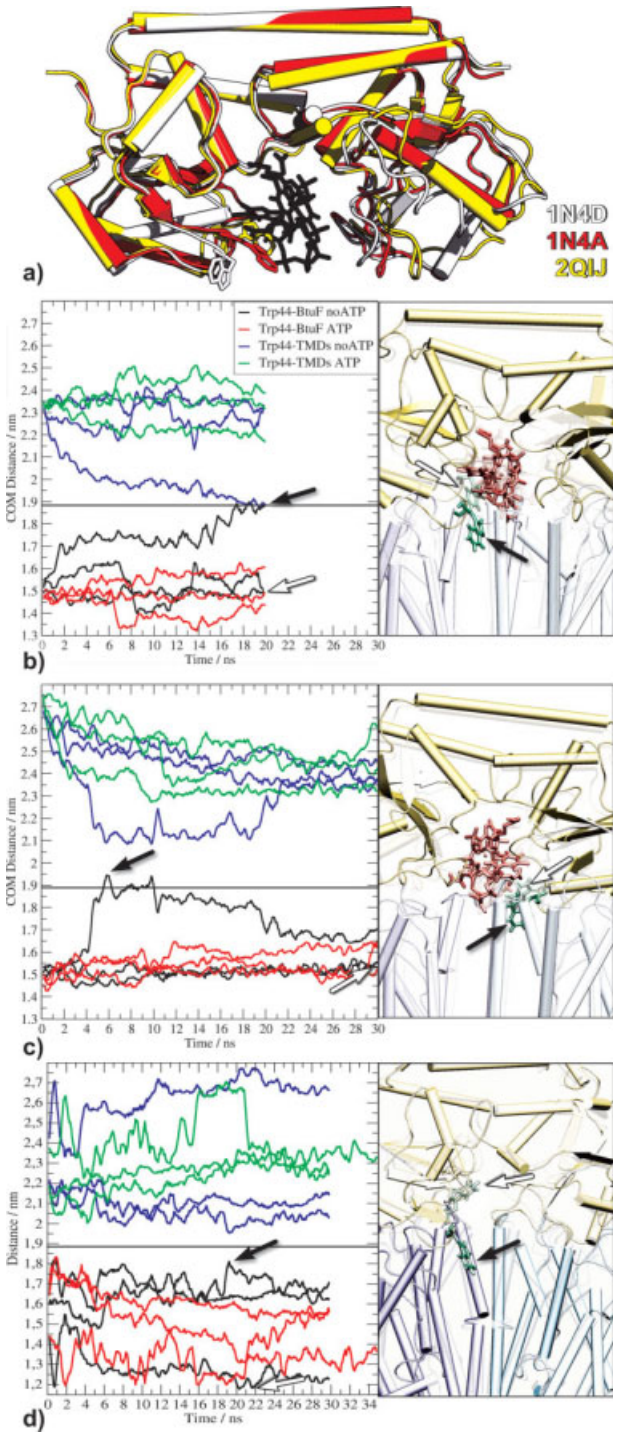

Figure 8

In the BtuF X-ray structures (**a**), Trp-44 faces toward vitamin B12 in holo-BtuF (red), away from the binding cleft in apo-BtuF (white) and adopts a cleft-facing conformation in the BtuCD-F crystal structure (yellow). As monitored by center of mass distances, in one of the nucleotide-free holocomplex 1 simulations (**b**), BtuF Trp 44 penetrates deeply into the BtuC transmembrane channel. A similar event is observed during the holocomplex 2 simulations (**c**) although here BtuF Trp44 relaxes back to a nonintruding position. A comparable event is also seen in apocomplex 1, but here the relaxation is not complete as the TMDs have closed trapping Trp44 in the protruding orientations (**d**). The arrows in the graphs refer to the simulation snap shots shown on the right: black arrows correspond to the opaque conformations; white arrows correspond to the translucent conformations.

docking approach, we used the unmodified BtuCD[7] and B12-bound BtuF crystal structures[31] to perform a two step steered docking search, where the only manual intervention is a 180° rotation of BtuF exploring the possibility of an alternate orientation of the binding protein.

Although the BtuF orientation in complex 1 coincides with the recently published apo-BtuCD-F crystal structure,[6] (Fig. 2), no experimental data have been reported yet for the second docking orientation. This could mean that a complex 2 orientation is either too short-lived or unstable under crystallization conditions and has therefore not been seen yet or does not occur *in vivo* at all. However, the latter possibility seems unlikely unless BtuF is permanently bound to BtuCD (and even then BtuF would have to get there in the first place), suggesting a complex 2 docking orientation could occur at least transiently. It will be interesting to see if further experiments will bring evidence supporting a complex 2 orientation, for instance via double spin-labeled EPR or fluorescence spectroscopy techniques.

If there is one favored orientation, as the apo-BtuCD-F X-ray structure and its crystallization conditions suggest, the transporter must have means to tell between the two BtuF orientations. This could for instance be done on grounds of vitamin B12 orientation in regard to the TMD uptake cleft. In that respect, it is remarkable that despite sharing only half of their interface residues before the simulations (Table II), both complexes apparently converge to the same set of BtuF and TMD interface residues by the end of the simulations (>70% common residues). These include more than 80% of the interface residues seen in the apo-BtuCD-F X-ray structure (Table III). On the other hand, the BtuCD-F complexes retain a different BSA which on average is lowest for complex 2 and highest for the B12-free complex 1, reaching levels equal to or exceeding the one in the apo-BtuCD-F crystal structure (Fig. 7). One must of course also bear in mind that simulation times are limited and both complexes might eventually very well reach the same level of TMD-BtuF interface area.

Holo-BtuF stabilizes an open transporter conformation

Open toward the periplasm, the BtuCD crystal structure[7] [Fig. 4(f)] displays a so-called outward facing conformation that is also seen in the X-ray structures of Sav1866,[22,23] HI1470/71,[19] and the full complex structure of MalGFK-E.[5] Embedded in a lipid/water environment, however, BtuCD closes within a few nanoseconds of unbiased MD simulation.[26,36] Deciding if a transporter is in an open or closed conformation requires a form of cavity analysis. There are different options available to identify cavities inside a protein and to determine if they are connected to the outside. Empty space inside a protein can be mapped by filling it with probe spheres of varying radius as in Refs. 70–72. This is particularly useful for single conformations or representative structures and bears the potential of obtaining pore or tunnel profiles assuming a circular cross section of the cavities of interest.[71,72] Alternatively and especially in trajectory analysis, a cavity can also be characterized by the dynamics of, for example, water molecule inside it[64,65] or protein residues lining the cavity. To this end, the frames in a trajectory can be visualized all together in an overlay of conformations or they can be averaged into residence probabilities per volume element like in MPDs per Å^3. Here, we used both approaches to compute slices through BtuCD-F MPDs (Fig. 3) as well as visualizing the trajectories of TMD-TMD interface residues that are within 4 Å of the respective subunit (Fig. 4). As the MPD slices can only be shifted along the *x*-, *y*- or *z*-axes and the TIA provides additional information on the shape of central cavity, both analysis techniques complement each other, allowing for a higher accuracy in detecting the BtuCD open state.

In our simulations, the transporter retains an open conformation within the 20–30 ns simulation time, as long as vitamin B12-loaded BtuF is docked [Figs. 3 and 4(a,d)]. If holo-BtuF or vitamin B12 is removed, the transporter closes within 20–35 ns in 5/6 and 6/6 cases in complex 1 [Figs. 3 and 4(b,c); Supporting Information Figure S1) and 2/4 cases in complex 2 [Figs. 3 and 4(e)]. Apparently, holo-BtuF stabilizes a BtuCD conformation that is open to the periplasm, suggesting the transporter can tell if BtuF is present and if it carries vitamin B12. This also supported by the apo-BtuCD-F crystal structure, given that BtuF is empty here and the transporter is closed toward both cytoplasm and periplasm [Fig. 4(g)], which is a unique feature among the available full length ABC transporter structures. The structural elements responsible for the closure in the apo-BtuCD-F crystal structure are a tilted transmembrane helix 5 in subunit A and the adjacent sealing helices protruding deeply into the BtuF substrate binding cleft, where they would clash with vitamin B12 if any were present [Fig. 2(d)]. The same helices are also responsible for the opposite accessibility in the BtuCD[7] and HI1470/71[19] X-ray structures.[15] In our BtuCD-F simulation, we identified α-helices in the TMDs that act as hotspots of conformational change (Fig. 6). Maximum changes occur more often in subunit A than B, further supporting the asymmetry aspect in not only in BtuCD[6] but ABC transporters in general.[11] Most changes happen at transmembrane helices 5 and 3, the L-loops and the sealing helices. While TM5 together with TM10 lines the postulated transport channel, and TM3 is situated directly next to TM5, the sealing helices are at the periplasmic surface of BtuCD, flanking the presumed B12 uptake cleft. Given that in the apo-BtuCD-F crystal structure the SH occupy more than half of the BtuF vitamin B12 binding cleft, whereas in our holo-BtuCD-F simulations the SH are a hotspot of conformational change in the TMDs, we propose the sealing helices may act as a substrate sensor. Providing a simple

structural basis by which the ABC transporter could tell between loaded and empty BtuF. Such a mechanism of substrate sensing could prevent or at least minimize Mg ATP consumption in the absence of transport substrate—as observed within the context of substrate sensitivity experiments carried out on other ABC transporters.[37–42]

A possible experimental scenario to test this hypothesis could include BtuC-internal crosslinking experiments that would constrain the SH conformation and test if this influences BtuCD substrate sensitivity or ATP consumption. However, whereas reconstitution experiments on maltose, histidine and glycine betaine ABC transporters brought clear evidence for substrate sensitivity,[37–42] similar experiments performed on BtuCD-F suggested otherwise.[33] The authors attributed this to (1) BtuF not being capable of large scale conformational changes like other periplasmic binding proteins and (2) a strong observed binding affinity toward BtuCD, resulting in a BtuF permanently bound to the transporter. Meanwhile, new computational and experimental evidence has emerged demonstrating that BtuF is capable of opening and closing motions[6,35] and in our holo-BtuCD-F simulations, we also observe BtuF opening by up to 3 Å (Supporting Information Figure 1).

On the other hand, the hypothesis of a permanently bound BtuF requires further experimental testing. For example, one could think of marking the binding protein with fluorescence labels and investigate the distribution of fluorescence signals in vivo. BtuF and BtuCD could also be crosslinked to ensure a doubtless connection. Observable vitamin B12 transport under such conditions would then back the hypothesis of BtuF hardly ever leaving its ABC transporter. It is also possible that BtuCD interacts with other proteins *in vivo* which might prove essential for transport. TonB would be such a candidate given that it is not only known to be crucial for vitamin B12 transport,[32] but has also been identified as a binding partner for the BtuF homologue and ferrichrome binding protein FhuD.[34] Beyond that, the opposite binding orientation of vitamin B12 found in BtuB and BtuF[28] could also be seen as supporting the idea of only transient BtuF–BtuCD interactions.

Subunit orientations support MalK model

Initially proposed when the MalK crystal structure was solved,[25] the currently most widely supported model of ABC transporter functional mechanism assumes that ATP-driven dimerization of the NBDs is concurrent with a tilting motion of the TMDs toward an outward-facing conformation.[3,13,16,21,26] Our BtuCD-F simulations also support this model, as we find the same pattern of NBD and TMD motions [Fig. 4(a,c)]. However, unlike the findings in Ref. 26, we do not observe any apparent coupling between NBD and L-loop motions [Fig. 5(b)]. This could be related to the different technical approaches of steered MD in Ref. 26 and unbiased MD in this study. One could also argue that the coupling between NBDs and TMDs might have weakened during the BtuCD-F simulations and therefore uncorrelated L-loop dynamics is seen. Against this speaks the overall increase in BSA between neighboring subunits in all BtuCD-F simulations. Alternatively, it is also thinkable that the L-loops do not necessarily follow the motions of the NBDs that closely, when that motion is not enforced like in Ref. 26. The HI1470/1 crystal structure[19] is open toward the cytoplasm and has its NBDs further apart than in the BtuCD X-ray structure,[7] as one would expect according to the MalK model. However, despite different TMD orientation and NBD distance, there is no difference in terms of L-loop distance between HI1470/1 and BtuCD. This suggest that the L-loops might not act like a toggle switch that remains in its extreme positions while on or off.

The largest conformational changes in our simulations occur as rigid-body like motions of the NBD subunits approaching each other—regardless if Mg ATP is present or not [Figs. 2(c,d) and 5(a)]. While simulations of BtuCD,[36,47] isolated Btu components[47] and maltose transporter NBDs[49] saw a clear effect of Mg ATP promoting NBD closure, NBD closing was observed in B12-free BtuCD-F runs, regardless if nucleotide was present or not.[47] We make the same observation in our holo- and apo-BtuCD-F simulations: Mg ATP appears to have no effect on NBD distance and transporter open state. Given that Mg ATP is a challenging to parametrize accurately,[73] our findings could be attributed to a flawed Mg ATP topology used in our simulations. However, since the same Mg ATP force field parameters were also used in Refs. 36 and 49, this seems unlikely. In light of these findings further experimental work is needed to test whether the observed effect of Mg ATP is a simulation artifact, a time scale effect or a feature of the transporter in complex with the SBP.

Like in many other MD studies our simulations are limited by the achieved amount of conformational sampling - despite a total simulation time of over half a microsecond (Table I). Although multicopy MD[50] was used, each of our six BtuCD-F simulation systems was only sampled by three independent copies. This small sampling size becomes especially obvious in the small Cα-RMSDs [Fig. 2(c,d)] and in some of the large standard deviations seen in Figure 4. Either there is indeed that much fluctuation going on in the subunit orientations in BtuCD-F, or three independent copies per BtuCD-F simulation system is not enough to see convergence to sharper defined average values. On the other hand, the amount of simulation time we performed is clearly at the upper end of the spectrum of membrane protein simulations of comparable system sizes today. However, with a maximum of 35 ns per run, the simulation time is too short to predict equilibrated complex structures which would likely require microseconds to obtain. However, our strategy has been to perturb

systems and look at the response in the systems. Given that our simulation systems are strongly perturbed by the addition and removal of BtuF, vitamin B12 or Mg ATP, we therefore focus on the transporters immediate response providing further evidence to extrapolate on the question of BtuCD-F functional mechanism in general and BtuCD-F capability to substrate sensitivity in particular.

Another point one might raise concerns a potential force field dependency of the results, and that the vitamin B12-dependent opening and closing behavior, we observed might therefore be a force field artifact. A set of control simulations using the G53a6-GROMOS96 force field gave the same results for the apo-BtuCD-F complex 1 scenarios (Supporting Information Figure S1), demonstrating the results are not dependent on force field details.

BtuF Trp 44 might be important in the transport cycle

No direct substrate uptake is observed during the simulations. However, an interesting observation is made concerning BtuF residue Trp44. As also noted by Liu et al.[74] and apparently depending on the presence of vitamin B12, Trp44 faces toward B12 in holo-BtuF[31] but points away from the binding cleft in apo-BtuF[6,31] [Fig. 8(a)]. During one of the nucleotide-free holocomplex 1 simulations, BtuF Trp44 is found to protrude deeply into the BtuC transmembrane channel [Fig. 8(b)]. A similar event is observed for the holocomplex 2 simulations, but here the intrusion is of lesser depth and the tryptophan relaxes back to a nonintruding position [Fig. 8(c)]. For apocomplex 1, we see a comparable intrusion event in a nucleotide-free run, but without relaxing back to a nonintruding orientation [Fig. 8(d)], as here Trp44 became locked in that orientation by the TMDs closing toward the periplasm. Additionally, without vitamin B12, Trp44 is also exploring the interior of the BtuF substrate binding cleft as reflected by a larger range of COM distances. On its own, the simulation observation of Trp44 protruding into the TMD channel might not be enough to suggest Trp44 playing a role in the initial steps of B12 uptake. However, in combination with the apparently B12-dependent Trp44 orientation seen in the holo- and apo-BtuF crystal structures, the Trp44 intrusion in our simulations provides evidence enough to at least postulate such a hypothesis. It will be interesting to see, if mutagenesis studies will detect an influence of Trp44 mutants on BtuCD-F transport activity. If that is the case, Trp44 intrusion into the transport channel might indeed represent an initial step in vitamin B12 uptake.

CONCLUSIONS

We reported results of protein docking and MD simulation studies addressing the question how BtuF, vitamin B12, and Mg-ATP influence the open state of BtuCD and if the transporter is capable of telling between empty and loaded BtuF and thus of substrate sensitivity. Starting from the BtuCD and holo-BtuF crystal structures we found two holo-BtuCD-F docking complexes, differing by a 180° rotation of BtuF. Of these two, complex 1 coincides with the BtuF orientation reported in the recently published apo-BtuCD-F crystal structure.[6] Both complexes were embedded in a lipid/water environment to investigate their dynamics and response to the presence and absence of BtuF, vitamin B12, and Mg ATP in a subsequent series of 28 multicopy MD simulations. Although the apo-BtuCD-F X-ray structure is closed toward the periplasm, we find holo-BtuF stabilizing an open, that is, outward-facing conformation of BtuCD. When the binding protein or vitamin B12 is removed, the transporter begins to close again suggesting that BtuCD-F is capable of substrate sensitivity. During the simulations, the NBDs approach each other whereas the TMD exhibit an opening trend toward the periplasm. We identified BtuC TM helices 3, 5, the L-loops, and the sealing helices comprising BtuC residues 170–180 as hotspots of conformational change. On the basis of their dynamics during the simulations and their conformation in the apo-BtuCD-F X-ray structure, we propose the sealing helices to act as substrate sensors. Whereas in BtuF X-ray structures[7,31] Trp44 switches between conformations pointing toward or away from the vitamin B12 binding cleft, we observe Trp44 protruding into the presumed TMD transport channel in one of our holo-BtuCD-F simulations, which might represent an initial step in vitamin B12 uptake.

ACKNOWLEDGMENTS

The author thank Dr. K. Locher, B. Chu, E.P. Coll, and A. Moussatova for their discussions on this topic. C.K. is a junior research group leader and D.P.T. is an AHFMR Senior Scholar and CIHR New Investigator.

REFERENCES

1. Aller SG, Yu J, Ward A, Weng Y, Chittaboina S, Zhuo R, Harrell PM, Trinh YT, Zhang Q, Urbatsch IL, Chang G. Structure of P-glycoprotein reveals a molecular basis for poly-specific drug binding. Science 2009;323:1718–1722.
2. Higgins CF. Multiple molecular mechanisms for multidrug resistance transporters. Nature 2007;446:749–757.
3. Ward A, Reyes CL, Yu J, Roth CB, Chang G. Flexibility in the ABC transporter MsbA: alternating access with a twist. Proc Natl Acad Sci USA 2007;104:19005–19010.
4. Lippincott J, Traxler B. MalFGK complex assembly and transport and regulatory characteristics of MalK insertion mutants. J Bacteriol 1997;179:1337–1343.
5. Oldham ML, Khare D, Quiocho FA, Davidson AL, Chen J. Crystal structure of a catalytic intermediate of the maltose transporter. Nature 2007;450:515–521.
6. Hvorup RN, Goetz BA, Niederer M, Hollenstein K, Perozo E, Locher KP. Asymmetry in the structure of the ABC transporter-binding protein complex BtuCD-BtuF. Science 2007;317:1387–1390.

7. Locher KP, Lee AT, Rees DC. The *E. coli* BtuCD structure: a framework for ABC transporter architecture and mechanism. Science 2002;296:1091–1098.
8. Stefkova J, Poledne R, Hubacek JA. ATP-binding cassette (ABC) transporters in human metabolism and diseases. Physiol Res 2004; 53:235–243.
9. Higgins CF. ABC transporters: physiology, structure and mechanism—an overview. Res Microbiol 2001;152:205–210.
10. Nikaido H, Hall JA. Overview of bacterial ABC transporters. Methods Enzymol 1998;292:3–20.
11. Davidson AL, Dassa E, Orelle C, Chen J. Structure, function, and evolution of bacterial ATP-binding cassette systems. Microbiol Mol Biol Rev 2008;72:317–364; table of contents.
12. Davidson AL, Chen J. ATP-binding cassette transporters in bacteria. Annu Rev Biochem 2004;73:241–268.
13. Dawson RJP, Hollenstein K, Locher KP. Uptake or extrusion: crystal structures of full ABC transporters suggest a common mechanism. Mol Microbiol 2007;65:250–257.
14. Jones PM, George AM. The ABC transporter structure and mechanism: perspectives on recent research. Cell Mol Life Sci 2004;61: 682–699.
15. Moussatova A, Kandt C, O'Mara ML, Tieleman DP. ATP-binding cassette transporters in *Escherichia coli*. Biochim Biophys Acta 2008; 1778:1757–1771.
16. Oldham ML, Davidson AL, Chen J. Structural insights into ABC transporter mechanism. Curr Opin Struct Biol 2008;18:726–733.
17. Procko E, O'Mara ML, Bennett WFD, Tieleman DP, Gaudet R. The mechanism of ABC transporters: general lessons from structural and functional studies of an antigenic peptide transporter. FASEB J 2009;23:1287–1302.
18. Linton KJ, Higgins CF. Structure and function of ABC transporters: the ATP switch provides flexible control. Pflugers Arch 2007;453: 555–567.
19. Pinkett HW, Lee AT, Lum P, Locher KP, Rees DC. An inward-facing conformation of a putative metal-chelate-type ABC transporter. Science 2007;315:373–377.
20. Hollenstein K, Frei DC, Locher KP. Structure of an ABC transporter in complex with its binding protein. Nature 2007;446:213–216.
21. Gerber S, Comellas-Bigler M, Goetz BA, Locher KP. Structural basis of trans-inhibition in a molybdate/tungstate ABC transporter. Science 2008;321:246–250.
22. Dawson RJ, Locher KP. Structure of a bacterial multidrug ABC transporter. Nature 2006;443:180–185.
23. Dawson RJ, Locher KP. Structure of the multidrug ABC transporter Sav1866 from *Staphylococcus aureus* in complex with AMP-PNP. FEBS Lett 2007;581:935–938.
24. Kadaba NS, Kaiser JT, Johnson E, Lee A, Rees DC. The high-affinity *E. coli* methionine ABC transporter: structure and allosteric regulation. Science 2008;321:250–253.
25. Chen J, Lu G, Lin J, Davidson AL, Quiocho FA. A Tweezers-like motion of the ATP-binding cassette dimer in an ABC transport cycle. Mol Cell 2003;12:651–662.
26. Sonne J, Kandt C, Peters GH, Hansen FY, Jensen MO, Tieleman DP. Simulation of the coupling between nucleotide binding and transmembrane domains in the ATP binding cassette transporter BtuCD. Biophys J 2007;92:2727–2734.
27. Cherezov V, Yamashita E, Liu W, Zhalnina M, Cramer WA, Caffrey M. In meso structure of the cobalamin transporter. Btu B, at 195 A resolution. J Mol Biol 2006;364:716–734.
28. Chimento DP, Kadner RJ, Wiener MC. The *Escherichia coli* outer membrane cobalamin transporter BtuB: structural analysis of calcium and substrate binding, and identification of orthologous transporters by sequence/structure conservation. J Mol Biol 2003; 332:999–1014.
29. Shultis DD, Purdy MD, Banchs CN, Wiener MC. Outer membrane active transport: structure of the BtuB:TonB complex. Science 2006; 312:1396–1399.
30. Borths EL, Locher KP, Lee AT, Rees DC. The structure of *Escherichia coli* BtuF and binding to its cognate ATP binding cassette transporter. Proc Natl Acad Sci USA 2002;99:16642–16647.
31. Karpowich NK, Huang HH, Smith PC, Hunt JF. Crystal structures of the BtuF periplasmic-binding protein for vitamin B12 suggest a functionally important reduction in protein mobility upon ligand binding. J Biol Chem 2003;278:8429–8434.
32. Bassford PJ, Jr, Bradbeer C, Kadner RJ, Schnaitman CA. Transport of vitamin B12 in tonB mutants of *Escherichia coli*. J Bacteriol 1976;128:242–247.
33. Borths EL, Poolman B, Hvorup RN, Locher KP, Rees DC. In vitro functional characterization of BtuCD-F, the *Escherichia coli* ABC transporter for vitamin B12 uptake. Biochemistry 2005;44:16301–16309.
34. Carter DM, Miousse IR, Gagnon JN, Martinez E, Clements A, Lee J, Hancock MA, Gagnon H, Pawelek PD, Coulton JW. Interactions between TonB from *Escherichia coli* and the periplasmic protein FhuD. J Biol Chem 2006;281:35413–35424.
35. Kandt C, Xu Z, Tieleman DP. Opening and closing motions in the periplasmic vitamin B12 binding protein BtuF. Biochemistry 2006; 45:13284–13292.
36. Oloo EO, Tieleman DP. Conformational transitions induced by the binding of MgATP to the vitamin B12 ATP-binding cassette (ABC) transporter BtuCD. J Biol Chem 2004;279:45013–45019.
37. Ames GF, Liu CE, Joshi AK, Nikaido K. Liganded and unliganded receptors interact with equal affinity with the membrane complex of periplasmic permeases, a subfamily of traffic ATPases. J Biol Chem 1996;271:14264–14270.
38. Boos W, Lucht J. Periplasmic binding protein-dependent ABC transporters. In: Neidhardt F, editor. *Escherichia coli* and *Salmonella typhimurium*: cellular and molecular biology. Washington, DC: American Society for Microbiology; 1996.
39. Liu CE, Liu PQ, Ames GF. Characterization of the adenosine triphosphatase activity of the periplasmic histidine permease, a traffic ATPase (ABC transporter). J Biol Chem 1997;272:21883–21891.
40. Merino G, Boos W, Shuman HA, Bohl E. The inhibition of maltose transport by the unliganded form of the maltose-binding protein of *Escherichia coli*: experimental findings and mathematical treatment. J Theory Biol 1995;177:171–179.
41. Patzlaff JS, van der Heide T, Poolman B. The ATP/substrate stoichiometry of the ATP-binding cassette (ABC) transporter OpuA. J Biol Chem 2003;278:29546–29551.
42. Reich-Slotky R, Panagiotidis C, Reyes M, Shuman HA. The detergent-soluble maltose transporter is activated by maltose binding protein and verapamil. J Bacteriol 2000;182:993–1000.
43. Weng J, Ma J, Fan K, Wang W. The conformational coupling and translocation mechanism of vitamin B12 ATP-binding cassette transporter BtuCD. Biophys J 2008;94:612–621.
44. Wen PC, Tajkhorshid E. Dimer opening of the nucleotide binding domains of ABC transporters after ATP hydrolysis. Biophys J 2008; 95:5100–5110.
45. Kandt C, Oloo E, Tieleman D. Domain coupling in the ABC transporter system BtuCD/BtuF: molecular dynamics simulation, normal mode analysis and protein-protein docking. Saskatoon SK, Canada: IEEE Computer Society Press; 2007.
46. Jones PM, George AM. Nucleotide-dependent allostery within the ABC transporter ATP-binding cassette: a computational study of the MJ0796 dimer. J Biol Chem 2007;282:22793–22803.
47. Ivetac A, Campbell JD, Sansom MS. Dynamics and function in a bacterial ABC transporter: simulation studies of the BtuCDF system and its components. Biochemistry 2007;46:2767–2778.
48. Oloo EO, Kandt C, O'Mara ML, Tieleman DP. Computer simulations of ABC transporter components. Biochem Cell Biol 2006;84: 900–911.
49. Oloo EO, Fung EY, Tieleman DP. The dynamics of the MgATP-driven closure of MalK, the energy-transducing subunit of the maltose ABC transporter. J Biol Chem 2006;281:28397–28407.

50. Caves LS, Evanseck JD, Karplus M. Locally accessible conformations of proteins: multiple molecular dynamics simulations of crambin. Protein Sci 1998;7:649–666.
51. Chen R, Li L, Weng Z. ZDOCK: an initial-stage protein-docking algorithm. Proteins 2003;52:80–87.
52. Chen R, Weng ZP. Docking unbound proteins using shape complementarity, desolvation, and electrostatics. Proteins: Struct Funct Genet 2002;47:281–294.
53. Ritchie DW, Kemp GJL. Protein docking using spherical polar Fourier correlations. Proteins: Struct Funct Genet 2000;39:178–194.
54. Berendsen HJC, Vanderspoel D, Vandrunen R. Gromacs—a message-passing parallel molecular-dynamics implementation. Comput Phys Commun 1995;91:43–56.
55. Lindahl E, Hess B, van der Spoel D. GROMACS 3.0: a package for molecular simulation and trajectory analysis. J Mol Model 2001;7: 306–317.
56. Kandt C, Ash WL, Peter Tieleman D. Setting up and running molecular dynamics simulations of membrane proteins. Methods 2007; 41:475–488.
57. Berendsen HJC, Postma JPM, Vangunsteren WF, Hermans J. Interaction models for water in relation to protein hydration. In: Pullman B, editor. Intermolecular forces. Dordrecht: Reidel; 1981. pp 331–342.
58. Hess B, Bekker H, Berendsen HJC, Fraaije JGEM. LINCS: a linear constraint solver for molecular simulations. J Comput Chem 1997; 18:1463–1472.
59. Berendsen HJC, Postma JPM, Vangunsteren WF, Dinola A, Haak JR. Molecular-dynamics with coupling to an external bath. J Chem Phys 1984;81:3684–3690.
60. Darden T, York D, Pedersen L. Particle Mesh Ewald—an n. log(n) method for Ewald sums in large systems. J Chem Phys 1993;98: 10089–10092.
61. Essmann U, Perera L, Berkowitz ML, Darden T, Lee H, Pedersen LG. A smooth particle Mesh Ewald method. J Chem Phys 1995;103: 8577–8593.
62. Oostenbrink C, Villa A, Mark AE, van Gunsteren WF. A biomolecular force field based on the free enthalpy of hydration and solvation: the GROMOS force-field parameter sets 53A5 and 53A6. J Comput Chem 2004;25:1656–1676.
63. Hess B, Kutzner C, van der Spoel D, Lindahl E. GROMACS 4: algorithms for highly efficient, load-balanced, and scalable molecular simulation. J Chem Theory Comput 2008;4:435–447.
64. Kandt C, Gerwert K, Schlitter J. Water dynamics simulation as a tool for probing proton transfer pathways in a heptahelical membrane protein. Proteins 2005;58:528–537.
65. Kandt C, Schlitter J, Gerwert K. Dynamics of water molecules in the bacteriorhodopsin trimer in explicit lipid/water environment. Biophys J 2004;86:705–717.
66. Humphrey W, Dalke A, Schulten K. VMD: visual molecular dynamics. J Mol Graph 1996;14:33–38, 27–38.
67. Hubbard S, Thornton J. NACCESS. Department of Biochemistry and Molecular Biology, University College London; 1993.
68. Sayle RA, Milner-White EJ. RASMOL: biomolecular graphics for all. Trends Biochem Sci 1995;20:374–376.
69. DeLano WL. The PyMol molecular graphics system. San Carlos, CA: DeLano Scientific; 2002.
70. Laskowski RA. SURFNET: a program for visualizing molecular surfaces, cavities, and intermolecular interactions. J Mol Graph 1995;13:323–330, 307–328.
71. Petrek M, Otyepka M, Banas P, Kosinova P, Koca J, Damborsky J. CAVER: a new tool to explore routes from protein clefts, pockets and cavities. BMC Bioinform 2006;7:316–324.
72. Smart OS, Neduvelil JG, Wang X, Wallace BA, Sansom MS. HOLE: a program for the analysis of the pore dimensions of ion channel structural models. J Mol Graph 1996;14:354–360, 376.
73. Liao JC, Sun S, Chandler D, Oster G. The conformational states of Mg.ATP in water. Eur Biophys J 2004;33:29–37.
74. Liu M, Sun T, Hu J, Chen W, Wang C. Study on the mechanism of the BtuF periplasmic-binding protein for vitamin B12. Biophys Chem 2008;135:19–24.